Programmable Sub-nanometer Sculpting of Graphene with Electron Beams

Felix Börrnert,[†] Lei Fu,[‡] Sandeep Gorantla,[†] Martin Knupfer,[†] Bernd Büchner,[†] and Mark H. Rümmeli*[,§]

[†]IFW Dresden, PF 27 01 16, 01171 Dresden, Germany, [‡]College of Chemistry and Molecular Science, Wuhan University, Wuhan 430072, China, and [§]Technische Universität Dresden, 01062 Dresden, Germany

ABSTRACT Electron beams in transmission electron microscopes are very attractive to engineer and pattern graphene toward all-carbon device fabrication. The use of condensed beams typically used for sequential raster imaging is particularly exciting since they potentially provide high degrees of precision. However, technical difficulties, such as the formation of electron beam induced deposits on sample surfaces, have hindered the development of this technique. We demonstrate how one can successfully use a condensed electron beam, either with or without C_s correction, to structure graphene with sub-nanometer precision in a programmable manner. We further demonstrate the potential of the developed technique by combining it with an established route to engineer graphene nanoribbons to single-atom carbon chains.

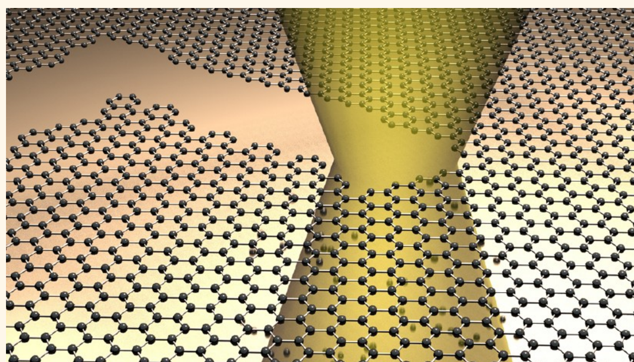

KEYWORDS: graphene · nanoribbon · sculpting · *in situ* TEM

Graphene nanostructures have drawn much attention for use in high-speed electronics.[1] Considerable advances in graphene synthesis make the production of all-carbon nanostructured devices ever closer.[2] To this end, great efforts have been made to calculate the electronic characteristics of different carbon nanostructures such as graphene nanoribbons and single carbon chains. For nanoribbons the electronic behavior is predicted to be dependent on the edge structure;[3] however, experiments to date have not confirmed such a dependency.[4] Single carbon chains are predicted to show either negative differential resistance, metallic, or semiconducting behavior, depending on their length.[5−8]

Experimentally correlating the electronic properties of graphene nanoribbons and single-atom carbon chains with their atomic structure requires an imaging tool that has sufficient spatial as well as temporal resolution. *In situ* electrical measurements within a transmission electron microscope (TEM) are an ideal choice for this task, since both atomic resolution and high temporal resolution are possible.[9] To achieve *in situ* electrical measurements in a TEM, the desired structures are best manufactured inside the TEM because their fragility as freely suspended nanostructures makes transfer between different instruments extremely difficult. The random production of structured nanocarbons inside a TEM has been reported.[8,10−12] However, the targeted and controlled manufacturing of sp^2 carbon nanostructures toward device fabrication inside the TEM is still lacking. To structure graphene efficiently with an electron beam, one has to use electrons with an energy above its knock-on damage threshold (*ca.* 86 keV).[13,14] In this regime atoms in the graphene lattice suffer a recoil energy transfer from the incoming high-energy electrons that is sufficient to break the bonds with all neighboring atoms and hence "knock" the atom out of the lattice. Below this threshold sputtering of atoms with unsaturated bonds from the edges is still possible since their knock-on threshold is reduced (*ca.* 50 keV).[9,15,16] One of the more challenging issues with focused electron beam lithographic routes is electron beam induced deposition (EBID) of amorphous carbon on the sample surface.[17] Here, residual hydrocarbons in the TEM column are cracked by the incoming high-energy

* Address correspondence to m.ruemmeli@ifw-dresden.de.

Received for review September 15, 2012 and accepted October 30, 2012.

Published online October 30, 2012
10.1021/nn304256a

© 2012 American Chemical Society

electrons of the imaging beam and adsorb on the surface of the sample. EBID is markedly worse when using condensed electron beam techniques such as scanning TEM (STEM). EBID can be reduced to some degree by improving vacuum operation conditions. Because of the formation of such deposits, there are only a few reports on structuring or manipulating carbon nanostructures directly with a *condensed* electron beam normally used for sequential raster imaging.

The drilling and cutting of carbon nanotubes (CNTs) has been shown in TEM mode for multiwalled CNTs[18−20] as well as in STEM mode with uncorrected[21] and C_s-corrected[22] condensor systems; however, all of these have been accomplished at elevated temperatures. For graphene, only TEM mode structuring has been reported.[23−25] In this route, single pores drilled in few-layer graphene were demonstrated. However, the technique affords limited spatial control and precision because of the imaging of the process; namely, the electron beam is not condensed. Carved lines have a minimum width of 20 nm,[23,25] and the adjacent material is highly damaged and requires annealing at temperatures of about 700 °C to recrystallize the heavily damaged material.[24] Current annealing may also be used in place of thermal annealing; however, current annealing results in even higher temperatures.[25] The need for annealing limits the technique since the elevated temperatures required would destroy other parts of the device. Moreover, sample drift is often a problem with heating stages. In general, the sculpting speed reported in these works is rather low. Other ways of structuring graphene such as catalytic etching,[26] current-induced cracking,[27] electron beam lithography,[4] scanning tunneling microscope lithography,[28] and others all lack precision and control and, more importantly, do not offer the combined *in situ* observation, measurement, and fabrication potential that TEM-based routes offer.

Here, we show that graphene nanoribbon/single carbon chain structures, potentially suitable for electrical characterization, can be fully manufactured in a controlled and reproducible manner inside a TEM. We develop an attractive route for electron beam sculpting in STEM mode (condensed beam) with sub-nanometer precision at convenient sculpting speeds, which does not damage the graphene or form EBID and so does not require high-temperature or current annealing during cutting. We demonstrate its potential to fabricate graphene constrictions. Thereafter the sculpting mode is switched to a selective beam sputtering mode in TEM mode, so that only edge atoms from the graphene are removed.[9,15] This already proven technique to structure graphene constrictions down to single carbon chains provides even higher degrees of precision, enabling easy and controlled nanoribbon shrinkage and single-atom carbon chain formation.[10,11] The combination of these two patterning/structuring modes provides an attractive platform to fully structure all-carbon devices inside a TEM. In addition, the performance of condensed electron beam sculpting (STEM) with a C_s-corrected condensor system is compared to that from an uncorrected condensor system.

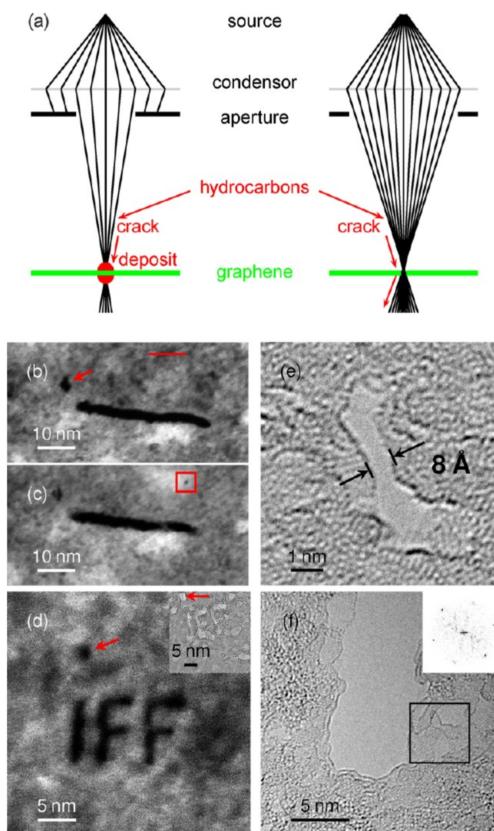

Figure 1. Precision sculpting with a C_s-corrected condensor system electron beam. (a) Schematic of a more conventional STEM setup showing the C_s-corrected electron beam projected through a small condenser aperture onto the graphene sample and the formation of electron-beam-induced deposits around the beam/sample interaction region (left) and the equivalent with a large condensor aperture where no deposits are formed (right). (b) DF STEM image of a successful single cut in graphene obtained with a 40 μm aperture. The red arrow indicates a hole formed at the rest position of the electron beam. The red line indicates the programmed track for another cut to sculpt. (c) Micrograph of the same area as in (b) after an unsuccessful cutting attempt with a 20 μm aperture. The red box shows the last position of the sculpting beam. (d) DF STEM image of "IFF" sculpted into graphene showing a structure size below 1 nm. The red arrow indicates a hole at the rest position of the electron beam. The inset is the corresponding TEM image. (e) TEM image of a cut in graphene with a width of 0.8 nm sculpted with a recently corrected electron beam and a 40 μm condensor aperture. (f) TEM image of a cut in graphene sculpted with a poorly C_s-corrected beam. The inset shows a FT of the region indicated by the black box.

RESULTS

Figure 1a contains two schematics highlighting the C_s-corrected condensed beam configurations explored for graphene sculpting. Panel (a) on the left provides a sketch of the electron beam path through the condensor and the sample in a conventional C_s-corrected

STEM arrangement. On the right, the modified system for sculpting is illustrated. In the conventional STEM arrangement one normally requires a small spot size to select only the electrons emitted at the very tip of the source so as to obtain a small electron probe as the image of the source (highest resolution). For sculpting, the largest spot size is required to provide the largest total current available. During imaging (normal STEM), a small condensor aperture is employed to restrict the beam within the best corrected area of the condensor system, since the C_s correction degrades as one deviates from the optical axis. In the case of sculpting, a large aperture is used, as this also enhances the total current of the electron probe. Hence, both the spot size and aperture selections used during sculpting enlarge the size of the spot (which decrease image resolution) but increase the total current. We employ high total currents, as our studies show this prevents EBID of amorphous carbon, which in turn allows us to successfully carve graphene. Examples of amorphous carbon deposits are provided in Figure S1(a) in the Supporting Information. Panel (b) of Figure 1 shows a dark field (DF) STEM image of few-layer graphene. The somewhat blotchy nature of the graphene image is due to the presence of some dirt on its surface. A dark line is clearly observed and indicates a single cut through the graphene sculpted with a 40 μm condensor aperture at an electron acceleration voltage of 200 kV. The C_s corrector alignment can drift slightly with time, which leads to a less than ideal spot and consequently cutting diameter. Due to this, the cut width in this example is slightly above 2 nm. The red arrow indicates the rest position of the electron beam. Panel (c) shows the same area after a sculpting attempt conducted along a preprogrammed track indicated in (b). The settings were the same except a 20 μm condensor aperture is used instead of 40 μm. The whiter contrast in its track is a clear signature of EBID of amorphous carbon since the observed contrast is dependent on the sample thickness. Only in the last point of the point series forming track is a hole observed (red box). This highlights the importance of aperture size selection and the need for high total currents to prevent EBID. In panel (d) the letters IFF (corresponding to our institute acronym: Insitut für Festkörperforschung) have been carved with a font size of 3×10^{-6} pt (10 nm) with a structure size of 1 nm. Again, the red arrow indicates the beam rest position. The inset shows a TEM image of the IFF carving, which also confirms the 1 nm cut width. Panel (e) shows a TEM image of a 0.8 nm wide cut in few-layer graphene, which represents our best cut-width resolution to date. This is accomplished by using a recently aligned and C_s-corrected probe. In contrast panel (f) shows a cut sculpted with a heavily drifted corrector alignment (*viz.*, poor C_s correction), where now the electrons in the beam are no longer ideally focused, yielding a broader cutting beam. Nevertheless, the micrograph nicely shows that no significant beam damage occurs when using a C_s-corrected probe, even when the C_s correction is not optimized. The inset shows a Fourier transform (FT) of the image from the region in the black box. It clearly shows six spots from the graphene lattice, indicating an intact crystal structure right at the edge of the cut. The exact mechanism as to how EBID is prevented so efficiently with high total currents (with a condensed C_s-corrected electron beam and large aperture selections) is an open question. We postulate that nearly all atoms of the cracked residual hydrocarbons are hit by the high-energy electrons of the beam and thus are able to obtain sufficient kinetic energy to avoid adsorption on the sample surface; namely, they have sufficient momentum to be ejected through the hole formed by the sculpting beam.

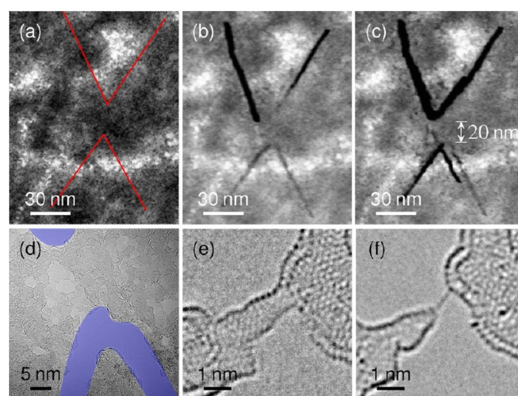

Figure 2. Manufacturing of a graphene nanoribbon/single carbon chain structure with a C_s-corrected condensor system/C_s-corrected objective lens electron beam. (a) DF STEM image of few-layer graphene sample. The red lines indicate the programmed track positions to be cut. (b) Micrograph of the same region after the first sculpting attempt with a cut speed of 1 nm s^{-1}. The procedure is seen to have been only partially successful due to deposit formation. (c) Micrograph of a second successful sculpting attempt with a cut speed of 0.5 nm s^{-1}, leaving a constriction of width 20 nm. (d) TEM image of the produced constriction after broad beam irradiation with 80 kV electrons. (e) Micrograph of a graphene nanoribbon produced out of the constriction by prolonged irradiation with 80 kV electrons. (f) Single carbon chain resulting from further irradiation of the graphene nanoribbon.

The efficiency of the annealing-free carving or sculpting condensed electron beam technique paves the way for damage-free sculpting of graphene and few-layer graphene over large lengths (m range) for suspended graphene or all-carbon device fabrication. Figure 2 demonstrates the controlled processing of a graphene nanoribbon/single carbon chain structure in which both coarse cutting with a condensed electron beam and fine sputter erosion with a broad electron beam at 80 kV are exploited to fabricate a nanoribbon out of a large graphene flake. The V-shaped cuts are chosen on the imaginary basis that the suspended graphene flake lies across two electrodes (left and right). Panel (a) shows a DF STEM image of few-layer

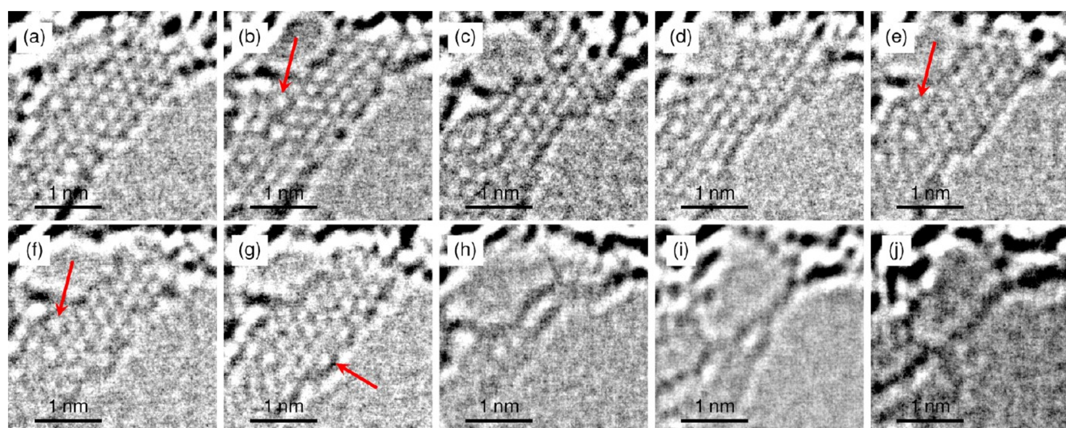

Figure 3. Evolution of a graphene ribbon under 80 kV broad beam electron irradiation. (a−g) Edge sputtering and reconstruction at the ribbon. (h−j) Development of a double carbon chain to a single carbon chain *via* an intermediate Y junction state.

graphene. The red lines indicate the programmed cutting path for the condensed electron beam to produce a constriction with a width of 20 nm. The cuts in panel (b) were obtained with a speed of 1 nm s^{-1} with an electron acceleration voltage of 200 kV. Contamination and sample drift prevented the complete cutting of the material; thus a second cut was programmed. This second cut was successful, yielding a 20 nm constriction as shown in panel (c). This shows a key advantage of *in situ* TEM-based sculpting, namely, that one rapidly sees the result and can correct, modify, or retry engineering strategies easily. In this case, the same cutting path was maintained; however, the cutting speed was reduced to 0.5 nm s^{-1}. To further reduce the constriction in a more refined manner, we exploit the selective sputtering of edge atoms as demonstrated in previous works.[9−11,15] In this mode the microscope is switched to the TEM imaging mode and the electron acceleration voltage reduced to 80 kV (*i.e.,* below the knock-on damage threshold of sp^2 carbon). Prior to the edge sputtering process the graphene was subjected to a "beam shower", which is a routine method to clean TEM specimens and in this case successfully removes any amorphous deposits on the surface of the graphene sample. This is important because amorphous material on sp^2 carbon has been shown to induce damage at acceleration voltages of 80 kV.[29] Panel (d) from Figure 2 shows the graphene specimen after this cleaning step. After cleaning, the few-graphene constriction is exposed to a conventional TEM beam. During this process the edge atoms sputter off, reducing the width of the constriction, and the number of layers thins down to a single layer to form a graphene nanoribbon as shown in panel (e) of Figure 2. During this engineering step the sputtering rate can be controlled by adjusting the beam intensity. Continuing the process ultimately leads to the formation of a single carbon chain. The carbon chain was stable under the electron beam for at least 24 s.

The slimming down of the graphene constriction is rich in terms of the restructuring processes involved. A variety of the reconstructions can be seen in Figure 3 and are in agreement with previous observations.[10,11] The edges can be seen to reconstruct over time and range from the smoothest zigzag form (*e.g.,* panel (e)) to jagged steps formed from a row of missing benzene rings (*e.g.,* panel (c)) and even carbon chains that form loops along the graphene edge (*e.g.,* panel (g)). Altered structures such as the presence of pentagons and heptagons are present and are relatively stable, again in agreement with previous observations[11] (see arrows in panels (b), (e), and (f)). At the end the ribbon narrows down to a double chain (panel (h)), which then forks (panel (i)) and then forms a single chain (panel (j)). A fuller overview of the process can be observed in movie M1 in the Supporting Information. Typically the carbon chains remain stable between 2 and 30 s. Another example of a fabricated graphene nanoribbon/single carbon chain using a C_s-corrected probe for initial constriction sculpting (200 kV) followed by TEM edge sputtering (80 kV) is shown in Figure S2 of the Supporting Information as well as a movie that nicely highlights the process over time (movie M2).

The use of a microscope *without* a C_s corrector for the condensor lens still encounters the same basic problem of EBID; however, it is difficult to attain the required high electron currents in the sculpting probe necessary to avoid deposit formation. This is because most of the electrons leaving the source are directed outside the central focal point on the sample plane of the condensed beam due to spherical aberrations. These stray electrons are effectively lost, and so the solution to avoid EBID must be fundamentally different. In the uncorrected system one normally inserts a condenser aperture in STEM mode to obtain a narrow beam (exactly as one does in the C_s-corrected system) (see Figure 4, panel (a), left side). This setup has a significantly reduced total current in the beam, and no

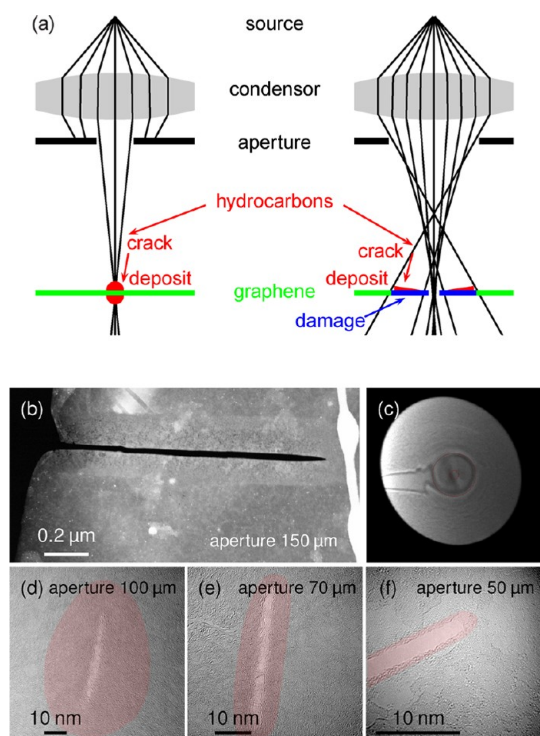

Figure 4. Sculpting with an uncorrected condensor system electron beam. (a) Schematic of an uncorrected electron beam projected through small condensor aperture onto the specimen (left) and with projection with a large condensor aperture (right). (b) DF STEM image of a single cut in graphene using a 150 μm aperture. (c) The corresponding Ronchigram while sculpting the cut shown in (b). (d) TEM image of a cut sculpted in graphene with a 100 μm condensor aperture inserted. The red-shaded area indicates the region where the graphene lattice is damaged by the electrons from the stray electrons (aberrated beam). (e) Same as in (d) but with an aperture of 70 μm. (f) Same as in (d) but with an aperture of 50 μm. The damaged region diminishes with smaller aperture use.

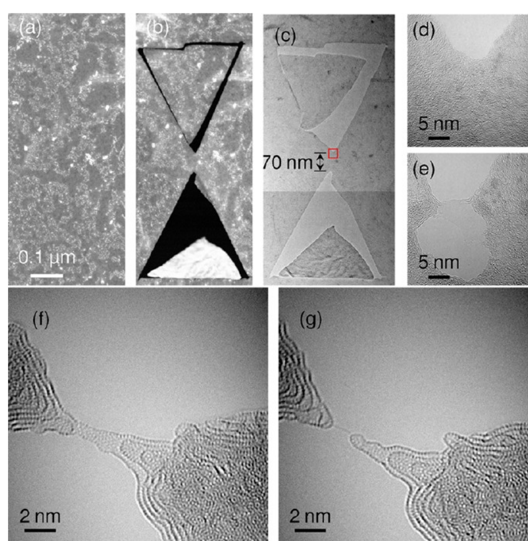

Figure 5. Manufacturing of a graphene nanoribbon/single carbon chain structure with an uncorrected condensor system/C_s-corrected objective lens electron beam. (a) DF STEM image of graphene sample. (b) Micrograph of the same region after sculpting with a cut speed of 0.3 nm s^{-1} and a condensor aperture of 100 μm. (c) TEM image of the produced structure. (d) Magnified section from (c) (red box) showing contamination from the STEM imaging process. (e) The same region as in (d) after "beam shower" cleaning with 80 kV electrons. (f) Micrograph of a graphene nanoribbon produced out of the constriction by prolonged irradiation with 80 kV electrons. (g) Single carbon chain from further irradiation to the graphene nanoribbon.

cutting or sculpting with the beam is possible. Instead, one simply builds deposits on the graphene surface. To enable cutting, we enlarge the aperture to increase the total cutting current just as we did for the C_s-corrected system. However, in this case we now have a spread of stray electrons surrounding the main central condensed beam as illustrated in Figure 4, panel (a), right side. The total current of the effective "cutting" beam is limited because stray electrons are lost. Nonetheless, these stray electrons turn out to be useful in terms of enabling cutting, because they form a curtain or surrounding electron shower that cracks hydrocarbons and deposits EBID, leaving the central effective cutting beam free to cut. This stray electron "curtain" suffers a drawback because it irradiates and damages the sample region surrounding the cut. Panel (b) shows a DF STEM image of a 2.5 μm long cut in multilayer graphene sculpted in 2 h 10 min with a 150 μm condensor aperture and an electron acceleration voltage of 300 kV. The cut is 20 nm wide. It is easy to observe the damage region surrounding the cut through the increased white contrast. This is more readily seen in Figure S1 of the Supporting Information. The damaged width is approximately 100 nm. Panel (c) shows a Ronchigram obtained during the cutting/patterning process. A Ronchigram is the shadow image of a specimen and directly reflects the characteristics of the specimen and the probe. In this case one sees a central blob or large spot with a tail. The tail represents the cutting track, and the central blob is the focused part of the electron beam that actually cuts the sample. The Ronchigram is very convenient because it provides real-time information to the operator with respect to the sculpting status. In the provided Ronchigram, one can also notice the beam image is asymmetric, and this is due the aperture not being perfectly centered on the beam; this explains the asymmetry of the damage region in panel (b). The lower row of panels (d)−(f) shows TEM images of cuts on multilayer graphene with condenser aperture sizes of 100, 70, and 50 m, respectively. This sample was relatively clean, so there was little problem with contamination; nonetheless the surrounding regions are damaged to varying degrees. The damage region is shaded red in the micrographs. The damage radius reduces nonlinearly from 100 nm for the largest aperture to minute edge damage for the smallest aperture. Greater detail on the edge structure of graphene after cutting is discussed later. The minimum cut width we were able to obtain with the uncorrected condensor system was 3 nm at a sculpting

speed of 0.1 nm s^{-1}. In both the C_s-corrected and uncorrected STEM systems we investigated if there was any preferential crystallographic direction for sculpting graphene. None was observed in either case.

As with the C_s-corrected condensor system, here we also explore the technique to pattern and structure graphene to a nanoribbon. Figure 5 shows DF STEM images of pristine few-layer graphene material (panel (a)) and after carving out two large triangles with a 300 kV uncorrected STEM sculpting setup (panels (b) and (c)). Note that the scale of the figures is four times larger than in Figure 2(a–c), which was made with a C_s-corrected condensor system. Moreover the remaining constriction is 70 nm wide as compared to 20 nm with the C_s-corrected system. This is because in order to obtain a damage-free region in the center of the constriction, one must choose a width larger than twice the damage radius. The total time to fabricating the constriction was 3 h 50 min. The potential of this method to carve even larger sections at the m scale is demonstrated in Figure S3 in the Supporting Information. Panel (c) shows the same region as panel (b), but recorded in TEM mode at 80 kV. Again, prior to the more spatially accurate engineering of the structure by edge sputtering at 80 kV in TEM mode, a "beam shower" was applied to clean the graphene surface. Panels (d) and (e) show the sample before and after the "beam shower", respectively. The depicted region is indicated by the red box in panel (c). Panels (f) and (g) show the fabricated graphene nanoribbon and eventual single carbon chain, respectively, after the edge sputtering process. We fabricated a number of these graphene nanoribbons and single carbon chains in both the C_s-corrected and uncorrected systems. Some eroded down directly to single carbon chains, while others would etch down to a pair of single carbon chains (see Figure S4 and movie M3 in the Supporting Information).

When comparing the C_s-corrected system *versus* the uncorrected, for the most part, having a probe C_s-corrected beam is advantageous. For example, when examining the quality of the cut edges, one sees that edges from the uncorrected system (after condensed beam cutting in STEM) are damaged, while those from the C_s-corrected setup are not. This is easily seen by comparing the two micrographs in Figure 6, which are taken from the most efficient cutting parameters for each of the two explored systems. The FT of the images are provided as insets. No reflex spots corresponding to a graphene lattice are observed for the sample from the uncorrected condensor system (left), while clear spots can be seen on the left image from the probe C_s-corrected cut, indicating the graphene crystal integrity is preserved. The edge roughness is 0.5 nm from the C_s-corrected and 0.7 nm for the uncorrected case (see Figure S5 in the Supporting Information). This level of edge precision compares very favorably with other

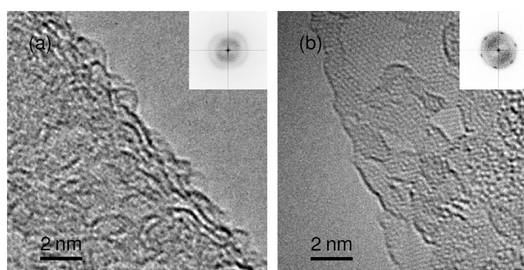

Figure 6. Comparison of the graphene edges resulting from optimized condensed electron beam sculpting with and without C_s correction. (a) TEM image of a cut edge sculpted with an uncorrected C_s beam with a 150 μm condensor aperture. The inset shows a FT of the image and shows no graphene lattice signal. (b) Micrograph of a cut edge sculpted with a C_s-corrected beam with a 40 μm condensor aperture. The inset shows a FT of the image indicating a clear graphene lattice signal.

TABLE 1. Comparison of the Main Characteristics of Annealing-Free Condensed Beam Sculpting with Uncorrected and C_s-Corrected Electron Beams, Respectively

condensor system	uncorrected	C_s-corrected
cut width	3 nm	0.8 nm
damage radius	0.5–100 nm[a]	none
cutting speed	0.3 nm s^{-1}	1 nm s^{-1}
edge roughness	0.7 nm	0.5 nm
annealing needed	no[b]	no

[a] Depends on aperture. [b] Yes, if recrystallization of the edges is required.

methods that do not involve annealing, *e.g.*, catalytic etching.[26]

Table 1 lists the main parameters for the carving from condensed beams in STEM for both the uncorrected and the C_s-corrected condensor system. In terms of cutting width, damage radius, cutting speed, and edge roughness, a C_s-corrected probe is clearly superior, much as one might expect. However, when graphene samples are heavily contaminated, it may be that the "curtain" of stray electrons is advantageous against EBID. While the difference in accelerating voltage was not evaluated in this study, we believe that any influence it may have is negligible, as both energies are well above the knock-on damage threshold and the sputtering rate difference for amorphous carbon is small.[30,31] Sculpting attempts with lower electron acceleration voltages between 80 and 100 kV showed no effect; namely, no cutting was obtained.

CONCLUSION

In conclusion, we demonstrate that damage-free sculpting of graphene with condensed electron beams is feasible. The developed technique does not require any additional thermal or current annealing treatments. We also demonstrate the technique works for both C_s-uncorrected and -corrected probes. C_s-corrected beams are shown to be superior in terms of accuracy and precision, unwanted surface deposition,

and cutting speed. Subnanometer edge precision is demonstrated for both C_s-corrected and uncorrected systems as well as large-scale sculpting in the μm range. The programmable cutting/sculpting process can be easily tracked, and corrections or adjustments by the user can be easily implemented. We demonstrate the potential of the technique for routine graphene engineering by preparing graphene constrictions, which upon changing TEM mode can be further engineered using a previously established technique to restructure the graphene nanoribbons to single-atom carbon chains. The use of our annealing-free sculpting route alone or in conjunction with other TEM-based methods advances the use of *in situ* TEM fabrication of all-carbon devices.

METHODS

For our studies, two types of graphene samples were used. In the first, natural graphite was sonicated in 1,2-dichlorethane and drop coated onto lacey carbon TEM grids. Subsequently, they were dried at 100 °C in dynamic vacuum at 10^{-3} Pa. This kind of sample is relatively clean but consists mostly of multilayer graphene with very few large graphene (μm sized) flakes. In the second, chemical vapor deposition synthesized graphene grown over Ni/Mo metal surfaces (see Dai *et al*. (2011)[32]) was transferred to holey carbon TEM grids. These samples provide large graphene flakes; however, the flakes tend to have higher levels of surface contamination due to the more complicated transfer process.

The microscope with a C_s-corrected condensor system was a JEOL JEM-2010F retrofitted with two CEOS third-order spherical aberration correctors for the objective lens (CETCOR) and the condensor system (CESCOR). For condensed beam based sculpting, the microscope was operated in STEM mode with an electron acceleration voltage of 200 kV and spot size *L*. The current in the electron probe is on the order of 10 nA, as estimated using an established Ronchigram image analysis method.[31] The beam position and residence time was controlled by a self-developed script for the Gatan DigitalMicrograph software through the Gatan DigiScan II system. For edge sputtering engineering of the graphene the microscope was operated in TEM mode with an electron acceleration voltage of 80 kV. The microscope with a non-C_s-corrected condensor was a FEI Titan 80-300 TEM with a CEOS CETCOR corrector for the objective lens. The annealing-free sculpting was done in STEM mode at an acceleration voltage of 300 kV with a spot size 1. The beam current readouts ranged from 0.2 nA with a 50 μm condensor aperture to 2.5 nA with a 150 μm condensor aperture. The beam current values provide only a rough estimate of the real beam current. The condensed beam was spatially controlled using the spectroscopy line profile function of the FEI TEM Imaging & Analysis software. For edge sputter etching the TEM mode was implemented with an electron acceleration voltage of 80 kV. All sculpting and imaging was done at room temperature. The TEM column vacuum pressures were around 10^{-5} Pa.

Conflict of Interest: The authors declare no competing financial interest.

Acknowledgment. We thank R. Träger for the rendering of the TOC image. We thank the SMWK (Project Number 13647) for financial support. F.B. acknowledges the DFG (RU1540/8-1); M. H.R. the EU (ECEMP) and the Freistaat Sachsen.

Supporting Information Available: Additional STEM images and intensity profiles from EBID contamination, TEM images from m scale cuts, and TEM images of more double and single carbon chains. TEM movies of various engineering processes are also provided. This material is available free of charge *via* the Internet at http://pubs.acs.org/.

REFERENCES AND NOTES

1. Geim, A. K. Graphene: Status and Prospects. *Science* **2009**, *324*, 1530–1534.
2. Rümmeli, M. H.; Rocha, C. G.; Ortmann, F.; Ibrahim, I.; Sevinçli, H.; Börrnert, F.; Kunstmann, J.; Bachmatiuk, A.; Pötschke, M.; Shiraishi, M.; *et al*. Graphene: Piecing it Together. *Adv. Mater.* **2011**, *23*, 4471–4490.
3. Son, Y.-W.; Cohen, M. L.; Louie, S. G. Energy Gaps in Graphene Nanoribbons. *Phys. Rev. Lett.* **2006**, *97*, 216803451–4.
4. Han, M. Y.; Özyilmaz, B.; Zhang, Y.; Kim, P. Energy Band-Gap Engineering of Graphene Nanoribbons. *Phys. Rev. Lett.* **2007**, *98*, 208605−1–4.
5. Lang, N. D.; Avouris, P. Oscillatory Conductance of Carbon-Atom Wires. *Phys. Rev. Lett.* **1998**, *81*, 3515–3518.
6. Tongay, S.; Senger, R.; Dag, S.; Ciraci, S. *Ab-initio* Electron Transport Calculations of Carbon Based String Structures. *Phys. Rev. Lett.* **2004**, *93*, 136404451–4.
7. Khoo, K. H.; Neaton, J. B.; Son, Y. W.; Cohen, M. L.; Louie, S. G. Negative Differential Resistance in Carbon Atomic Wire-Carbon Nanotube Junctions. *Nano Lett.* **2008**, *8*, 2900–2905.
8. Börrnert, F.; Börrnert, C.; Gorantla, S.; Liu, X.; Bachmatiuk, A.; Joswig, J.-O.; Wagner, F. R.; Schäffel, F.; Warner, J. H.; Schönfelder, R.; *et al*. Single-Wall-Carbon-Nanotube/Single-Carbon-Chain Molecular Junctions. *Phys. Rev. B* **2010**, *81*, 085439−1–5.
9. Warner, J. H.; Rümmeli, M. H.; Ge, L.; Gemming, T.; Montanari, B.; Harrison, N. M.; Büchner, B.; Briggs, G. A. D. Structural Transformations in Graphene Studied with High Spatial and Temporal Resolution. *Nat. Nanotechnol.* **2009**, *4*, 500–504.
10. Jin, C.; Lan, H.; Peng, L.; Suenaga, K.; Iijima, S. Deriving Carbon Atomic Chains from Graphene. *Phys. Rev. Lett.* **2009**, *102*, 205501−1–4.
11. Chuvilin, A.; Meyer, J. C.; Algara-Siller, G.; Kaiser, U. From Graphene Constrictions to Single Carbon Chains. *New J. Phys.* **2009**, *11*, 083019−1–10.
12. Chuvilin, A.; Bichoutskaia, E.; Gimenez-Lopez, M. C.; Chamberlain, T. W.; Rance, G. A.; Kuganathan, N.; Biskupek, J.; Kaiser, U.; Khlobystov, A. N. Self-Assembly of a Sulphur-Terminated Graphene Nanoribbon Within a Single-Walled Carbon Nanotube. *Nat. Mater.* **2011**, *10*, 687–692.
13. Smith, B. W.; Luzzi, D. E. Electron Irradiation Effects in Single Wall Carbon Nanotubes. *J. Appl. Phys.* **2001**, *90*, 3509–3515.
14. Meyer, J. C.; Chuvilin, A.; Kaiser, U. Graphene − Two-dimensional Carbon at Atomic Resolution. *MC2009* **2009**, *3*, 347–348.
15. Girit, Ç. Ö.; Meyer, J. C.; Erni, R.; Rossell, M. D.; Kisielowski, C.; Yang, L.; Park, C.-H.; Crommie, M. F.; Cohen, M. L.; Louie, S. G.; *et al*. Graphene at the Edge: Stability and Dynamics. *Science* **2009**, *323*, 1705–1708.
16. Kotakoski, J.; Santos-Cottin, D.; Krasheninnikov, A. V. Stability of Graphene Edges under Electron Beam: Equilibrium Energetics versus Dynamic Effects. *ACS Nano* **2012**, *6*, 671–676.
17. Williams, D. B.; Carter, C. B. *Transmission Electron Microscopy*; Plenum Press: New York, 1996.
18. Li, J.; Banhart, F. The Engineering of Hot Carbon Nanotubes with a Focused Electron Beam. *Nano Lett.* **2004**, *4*, 1143–1146.
19. Banhart, F.; Li, J.; Terrones, M. Cutting Single-Walled Carbon Nanotubes with an Electron Beam: Evidence for Atom Migration Inside Nanotubes. *Small* **2005**, *1*, 953–956.
20. Aref, T.; Remeika, M.; Bezryadin, A. High-Resolution Nanofabrication Using a Highly Focused Electron Beam. *J. Appl. Phys.* **2008**, *104*, 024312-1–6.
21. Zobelli, A.; Gloter, A.; Ewels, C. P.; Colliex, C. Shaping Single Walled Nanotubes with an Electron Beam. *Phys. Rev. B* **2008**, *77*, 045410−1–8.

22. Rodríguez-Manzo, J. A.; Banhart, F. Creation of Individual Vacancies in Carbon Nanotubes by Using an Electron Beam of 1 Å Diameter. *Nano Lett.* **2009**, *9*, 2285–2289.
23. Fischbein, M. D.; Drndić, M. Electron Beam Nanosculpting of Suspended Graphene Sheets. *Appl. Phys. Lett.* **2008**, *93*, 113107−1–3.
24. Song, B.; Schneider, G. F.; Xu, Q.; Pandraud, G.; Dekker, C.; Zandbergen, H. Atomic-Scale Electron-Beam Sculpting of Near-Defect-Free Graphene Nanostructures. *Nano Lett.* **2011**, *11*, 2247–2250.
25. Lu, Y.; Merchant, C. A.; Drndić, M.; Johnson, A. T. C. In Situ Electronic Characterization of Graphene Nanoconstrictions Fabricated in a Transmission Electron Microscope. *Nano Lett.* **2011**, *11*, 5184–5188.
26. Schäffel, F.; Wilson, M.; Bachmatiuk, A.; Rümmeli, M. H.; Queitsch, U.; Briggs, B. R. G. A. D.; Warner, J. H. Atomic Resolution Imaging of the Edges of Catalytically Etched Suspended Few-Layer Graphene. *ACS Nano* **2011**, *5*, 1975–1983.
27. Barreiro, A.; Börrnert, F.; Rümmeli, M. H.; Büchner, B.; Vandersypen, L. M. K. Graphene at High Bias: Cracking, Layer by Layer Evaporation, and Fusing. *Nano Lett.* **2012**, *12*, 1873–1878.
28. Tapasztó, L.; Dobrik, G.; Lambin, P.; Biró, L. P. Tailoring the Atomic Structure of Graphene Nanoribbons by Scanning Tunnelling Microscope Lithography. *Nat. Nanotechnol.* **2008**, *3*, 397–401.
29. Warner, J. H.; Schäffel, F.; Zhong, G.; Rümmeli, M. H.; Büchner, B.; Robertson, J.; Briggs, G. A. D. Investigating the Diameter-Dependent Stability of Single-Walled Carbon Nanotubes. *ACS Nano* **2009**, *3*, 1557–1563.
30. Banhart, F. Irradiation Effects in Carbon Nanostructures. *Rep. Prog. Phys.* **1999**, *62*, 1181–1221.
31. Egerton, R. F.; Wang, F.; Crozier, P. A. Beam-Induced Damage to Thin Specimens in an Intense Electron Probe. *Microsc. Microanal.* **2006**, *12*, 65–71.
32. Dai, B.; Fu, L.; Zou, Z.; Wang, M.; Xu, H.; Wang, S.; Liu, Z. Rational Design of a Binary Metal Alloy for Chemical Vapour Deposition Growth of Uniform Single-Layer Graphene. *Nat. Commun.* **2011**, *2*, 522.